Rock and Soil Mechanics

Volume 42 | Issue 6 Article 5

10-22-2021

A new solution to the ultimate bearing capacity of reinforced ground near slope based on the unified strength theory

Qing YAN

Jun-hai ZHAO

Chang-guang ZHANG
zcg1016@163.com

Follow this and additional works at: https://rocksoilmech.researchcommons.org/journal

 Part of the Geotechnical Engineering Commons

Custom Citation
YAN Qing, ZHAO Jun-hai, ZHANG Chang-guang. A new solution to the ultimate bearing capacity of reinforced ground near slope based on the unified strength theory[J]. Rock and Soil Mechanics, 2021, 42(6): 1587-1600.

This Article is brought to you for free and open access by Rock and Soil Mechanics. It has been accepted for inclusion in Rock and Soil Mechanics by an authorized editor of Rock and Soil Mechanics.

Rock and Soil Mechanics 2021 42(6): 1587−1600 ISSN 1000−7598
https: //doi.org/10.16285/j.rsm.2020.6861 rocksoilmech.researchcommons.org/journal

A new solution to the ultimate bearing capacity of reinforced ground near slope based on the unified strength theory

YAN Qing, ZHAO Jun-hai, ZHANG Chang-guang
School of Civil Engineering, Chang'an University, Xi'an, Shaanxi 710061, China

Abstract: In view of two modes of general shear failure and composite failure of reinforced ground, a new solution to the ultimate bearing capacity of strip footings resting on reinforced ground near slope was derived based on the unified strength theory and the application procedures were given. Effects of the intermediate principal stress, the vertical spacing between reinforced material layers, the number of reinforced material layers, and the tensile strength of reinforced materials were comprehensively taken into consideration in the new solution. Compared with other methods, the effectiveness and parameter influence characteristics of the proposed method were discussed. The results showed that the obtained solution to the ultimate bearing capacity of reinforced ground agreed well with the results of model tests reported in the literature, and it had wide applicability. With the increase of the effect of intermediate principal stress, the ultimate bearing capacity of reinforced ground near slope subjected to general shear failure and composite failure increased markedly. As the vertical spacing between reinforced material layers increased, the ultimate bearing capacity of reinforced ground near slope increased first and then decreased under the general shear failure, but it would gradually reduce under the composite failure. The influence of the number of reinforced layers under the general shear failure can be divided into three stages, and that under the composite failure can be divided into two stages. Meanwhile, the effect of the tensile strength of reinforced materials cannot be ignored. The research results can provide useful references for the optimization design of reinforced ground near slope.

Keywords: reinforced ground near slope; ultimate bearing capacity; unified strength theory; general shear failure; composite failure

1 Introduction

It is one of the effective methods to reinforce the ground by placing single or multi-layer reinforced materials in the soil below the footing[1−4]. In the previous literatures[5−9], the results of some model tests suggested that reinforcement technology can effectively improve the bearing capacity of the ground, and there are two main failure modes of reinforced ground, i.e., the general shear failure, and the composite failure incorporating punching shear failure of soil in reinforced area and general shear failure of soil under reinforced materials. Based on the failure mode of Prandtl's ground, Liang et al.[10] deduced the solution of limit equilibrium method for ultimate bearing capacity of single-layer reinforced sandy soil by taking the transition zone as an isolation body, and considering the friction force between the reinforced materials and soils. Liu et al.[11] and Cao et al.[12] obtained the expression of ultimate bearing capacity of the reinforced ground through the slices method and critical slip field method based on the assumption that the reinforced ground was subjected to a general shear failure mode. Sharma et al.[13] and Chen et al.[14] obtained the solutions to the ultimate bearing capacity of reinforced ground in the case of general shear failure and composite failures by using limit equilibrium method.

The theoretical studies on the ultimate bearing capacity of reinforced ground described above are all aimed at horizontal ground. At present, the geosynthetics reinforcement technique has been widely applied in the reinforcement of ground adjacent to slope. Many researchers have carried out model tests and finite element numerical simulation on the bearing capacity. For example, in some previous studies, model tests were used to investigate the influence of parameters of reinforced material on the ultimate bearing capacity of strip footings on sandy slope[15−17]. Ma et al.[18] studied the effect of the number of reinforced layers and the buried depth of reinforced layers on the ultimate bearing capacity and failure modes of reinforced sand slope through model tests, and proposed three types of soil failure modes above, between and below the reinforced layers. Sommers et al.[19] simulated the in-situ conditions in the field and carried out the model tests on behavior of strip footing near slope by using the large-scale beam centrifuge. Through digital image analysis, they obtained the strain distribution of the reinforced layers

Received: 12 December 2020 Revised: 8 April 2021
This work was supported by the National Natural Science Foundation of China(51878056), the Social Development Foundation for Science and Technology Planning Project of Shaanxi Province (2019SF-256), the Opening Fund of State Key Laboratory of Geohazard Prevention and Geoenvironment Protection (SKLGP2020K022) and the Fundamental Research Funds for the Central Universities of Chang'an University(300102289720).
First author: YAN Qing, female, born in 1992, PhD candidate, mainly engaged in the research of strength theory and application in geotechnical engineering. E-mail: yanqing1210@126.com
Corresponding author: ZHANG Chang-guang, male, born in 1982, PhD, Professor, mainly engaged in unsaturated soil and underground engineering teaching and research work. E-mail: zcg1016@163.com

under different loading pressures. Shin et al.[20] conducted the undrained model test on the strip footing on a reinforced clay slope and discussed the reinforcement effect on the ultimate bearing capacity of the ground. Combined with finite difference method and random field model, Halder et al.[21] obtained the influence of spatial variability and randomness of soil strength parameters on the load−settlement characteristics of the strip footing on geocell-reinforced slope. The above studies suggest that the bearing capacity of the reinforced ground near slope is significantly improved, and most of the failure occurs on the side adjacent to the slope. Previous research results of model test and numerical simulation on the failure modes and bearing characteristics of the reinforced ground near slope provide a reference for the determination of bearing capacity, but there are few theoretical studies on the solution of ultimate bearing capacity of the reinforced ground near slope. Only Jha et al.[22] proposed a formula of ultimate bearing capacity of the fly ash reinforced slope when the strip footing was placed on the top of slope by using the stress balance of the reinforced layer.

In the past, Mohr-Coulomb strength criterion was always adopted to calculate the ultimate bearing capacity of the ground near slope or the horizontally reinforced ground without considering the effect of intermediate principal stress on the strength of foundation soil[23−25]. However, the intermediate principal stress has an obvious effect on the strength of soil, and the calculation of soil strength without considering the effect of intermediate principal stress is conservative[26−27]. The unified strength theory is a set of strength criteria proposed by Yu[28−29] based on the twin shear element model. It has been widely used in determining the ultimate bearing capacity of unreinforced horizontal ground[30−33] because reasonably considering the influence of intermediate principal stress σ_2 on soil strength. In this paper, based on the unified strength theory, the influences of intermediate principal stress and reinforcement parameters (the vertical spacing between reinforced material layers, the number of reinforced materiallayers, and the tensile strength of reinforcements) are discussed. Assuming that there are two main failure modes of reinforced ground, i.e. general shear failure and composite failure, the solution of ultimate bearing capacity of reinforced ground near slope is derived by using unilateral sliding surface, and the application steps are given in detail. The effectiveness of the solution is verified by comparing with other methods and the model test results. Finally, the influence of various parameters on the ultimate bearing capacity of reinforced ground near slope is discussed.

2 Fundamental assumption

For a rigid strip footing near the slope, the multi-layer geosynthetics were applied to the soil below, where the width of footing is B, the buried depth of footing is D, the slope angle is η, and the ultimate bearing capacity of the soil is q_{ur} when the soil is in the ultimate equilibrium state. Based on the model test results in the literatures[15, 18−19], there are four possible failure modes of reinforced ground near slope, as shown in Fig.1. Figure 1(a) shows the failure above the reinforced material layers, which usually occurs when the distance between footing bottom and top layer of reinforced materials $u>0.5B$[18]. Figure 1(b) shows the failure between layers of reinforced materials, which usually occurs when $u\leqslant 0.5B$, while the vertical spacing between reinforced material layers $z_i>0.5B$[18]. Figure 1(c) shows the general shear failure, which usually occurs in the sandy soil ground with a large distance h_n between the bottom layer of reinforced materials and footing bottom[15, 19]. Figure 1(d) shows the composite failure, in which the punching shear failure occurs in the soil within h_n, and the general shear failure occurs in the soil below the reinforced zone. This situation (Fig.1(d)) usually occurs in the clay ground or sandy soil ground with a smaller h_n[18]. The reinforcement effect of reinforced materials under the two failure modes shown in Figs. 1(a) and 1(b) cannot be fully exerted. It is pointed out in the literatures[13−14, 34] that controlling the distance between footing bottom and top layer of reinforced materials $u\leqslant 0.5B$ and the vertical spacing between reinforced material layers $z_i\leqslant 0.5B$ can avoid the occurrence of these two failure modes. Therefore, under the condition of $u\leqslant 0.5B$ and $z_i\leqslant 0.5B$, we deduced the formula of ultimate bearing capacity of reinforced ground near slope based on the two failure modes shown in Figs. 1(c) and 1(d).

The calculation model of reinforced ground in case of general shear failure is shown in Fig.2, which is composed of three parts: region I, region II and region III. The calculation model of reinforced ground in case of composite failure is shown in Fig.3, which consists of four parts: regions I, II, III, and IV. In the actual projects, the failure of reinforced ground near slope might occur in two cases in Fig.2 and Fig.3: when the DF plane is inclined downward, the included angle α between the DF plane and the horizontal plane is positive, and the deepest point of the slip line appears at point F in region III; while when the DF plane is inclined upward, the included angle α between the DF plane and the horizontal plane is negative, and the deepest point of the slip line appears on the CD plane in region II. In the following, the ultimate bearing capacity of the reinforced ground near slope is

solved according to Fig.2 and Fig.3, and several fundamental assumptions are made:

(1) The bottom surface of the footing is completely smooth, the soil within the buried depth D can be simplified as an equivalent uniform load q, i.e., $q = \gamma D$ (γ is the unit weight of soil). L is the horizontal distance from the footing to the slope shoulder, which can be expressed as $L=aB$ (a is the distance coefficient, i.e., the ratio of distance L to footing width B).

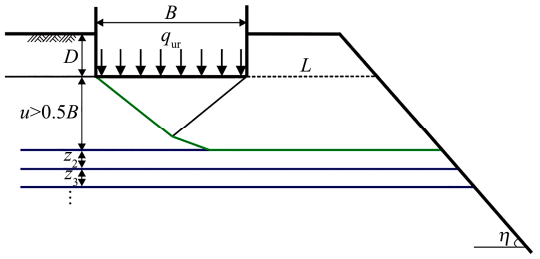

(a) Failure above reinforced material layers

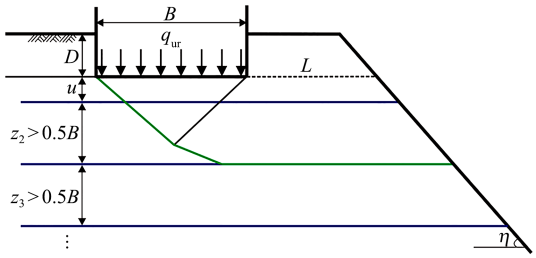

(b) Failure between reinforced material layers

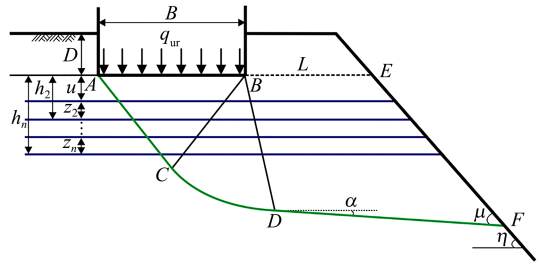

(c) General shear failure

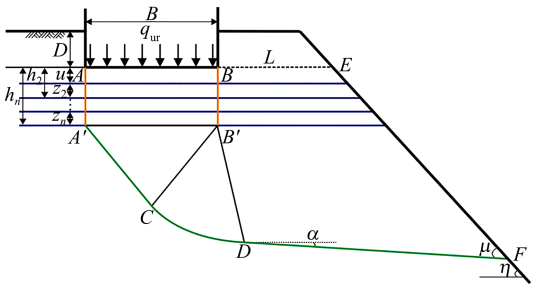

(d) Composite failure

Fig. 1 Failure modes of reinforced ground near slope

(2) When n layers of reinforced materials are horizontally arranged in the ground, and h_i (i = 2, ⋯, n) is the vertical distance from the i layer of reinforced materials to footing bottom, then the vertical spacing of reinforced

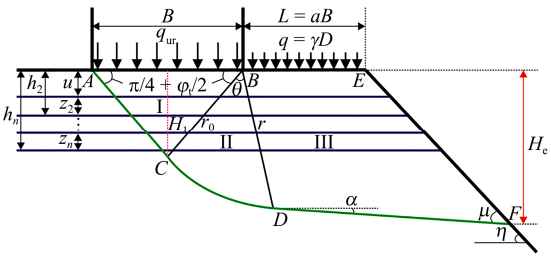

(a) $\alpha > 0$

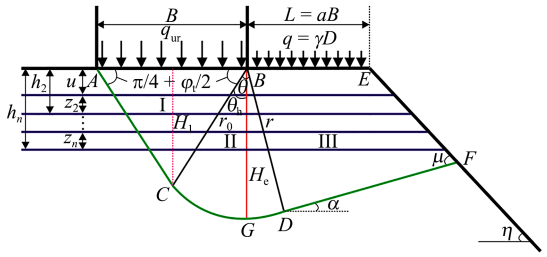

(b) $\alpha \leqslant 0$

Fig. 2 Calculation models for the general shear failure of reinforced ground near slope

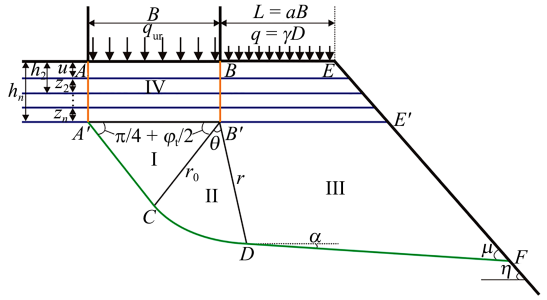

(a) $\alpha > 0$

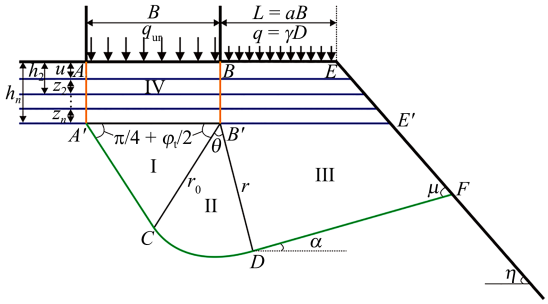

(b) $\alpha \leqslant 0$

Fig. 3 Calculation models for the composite failure of reinforced f ground near slope

materials is $z_i = h_i - h_{i-1}$. Assuming that the reinforced material is flexible, the influence of its bending stiffness on the bearing capacity of soil can be ignored, and only the tensile effect of reinforced materials is considered. When the ground fails, reinforced materials will break, and there is enough anchorage length not to be pulled out.

(3) Regions I, II and III in Figs. 2 and 3 are general shear failure regions. The soil near slope fails first. It is

assumed that the stress state of the soil on two footing sides is the same, so the region I is a symmetric elastic wedge, and the angle between planes BC and AB in Fig.2 (between planes $B'C$ and $A'B'$ in Fig.3) is $\pi/4+\varphi_t/2$. Region II is the shear transition region and CD is the logarithmic spiral. Region III is the Rankine passive region, and the angle between plane DF and the slope surface EF is $\mu=\pi/4-\varphi_t/2$. Region IV in Fig.3 is the punching shear failure region.

(4) The shear strength formula under plane strain state based on the unified strength theory is adopted to calculate the soil strength, which is expressed as[28−29, 35]:

$$\tau_f = c_t + \sigma\tan\varphi_t \tag{1}$$

where $\sin\varphi_t = \dfrac{2(1+b)\sin\varphi}{2+b(1+\sin\varphi)}$, $c_t = \dfrac{2(1+b)c\cos\varphi}{2+b(1+\sin\varphi)}\cdot\dfrac{1}{\cos\varphi_t}$.

In Eq.(1), σ is the compressive stress along the normal direction of the sliding surface; c is the cohesion; φ is the internal friction angle; c_t is the unified cohesion; φ_t is the unified internal friction angle; and b is the unified strength theoretical parameter, which reflects the intermediate principal stress effect on soil strength, and the value range is $0\leqslant b\leqslant 1$. Parameter b can also represent the selection of soil strength criterion. When $b=0$, Eq.(1) is degenerated into the classical shear strength formula of Mohr-Coulomb strength criterion. When b=1, Eq.(1) is the plane strain shear strength formula of the twin shear stress strength criterion. When $0<b<1$, a series of new shear strength formulas under plane strain state can be obtained.

3 New solutions to ultimate bearing capacity

The effect of reinforced materials on improving the ultimate bearing capacity of ground is mainly manifested as the 'membrane effect' of the vertical component and the 'lateral restraint effect' of the horizontal component of tensile force of reinforced materials[2, 12, 24]. As the load increases, the direction of tensile force T_r will change with the sliding deformation of soil. It is assumed that the soil is in the limit equilibrium state, the angle between the tensile force of reinforced material T_r and the horizontal plane is ξ. The tensile direction of reinforced material is related to its stiffness: when the stiffness of reinforced material is large, the tensile force is in the horizontal direction, but the economic cost is high, so it is rarely used in engineering practice[36]; when the stiffness is small, the tensile force is along the tangent direction of sliding surface. For the convenience of calculation, the suggestion from the previous study[2] is adopted in this paper, and $\xi=\pi/4+\varphi_t/2$, that is, the tensile force of reinforced material is along the tangent direction of the sliding surface AC in Fig.2 ($A'C$ in Fig.3). The tensile force of reinforced material T_r is taken as its allowable tensile strength, then

$$T_r = \frac{T_u}{RF} = \frac{T_u}{RF_{CR}RF_{ID}RF_D} \tag{2}$$

where T_u is the ultimate tensile strength of reinforced material; RF is the reduction coefficient of comprehensive strength; RF_{CR} is the creep reduction coefficient, and its value is between 2.5 and 5; RF_{ID} is the reduction coefficient of mechanical failure, and its value can reach 3; and RF_D is the aging reduction coefficient, which is generally equal to 2[37]. The range of creep reduction coefficient of commonly used geosynthetics are as follows[37−38]: polyester (PET) is between 2.5 and 3; polypropylene (PP) is between 4 and 5, and polyethylene (PE) is between 2.5 and 5.

According to the calculation models of reinforced ground near slope in Fig.2 and Fig.3, considering the influence of tension of reinforced material, the ultimate bearing capacity formulas of reinforced ground near slope under general shear failure mode and composite failure mode will be derived by using limit equilibrium method.

3.1 General shear failure

Since the two calculation models in Fig.2 do not affect the derivation process of the formula for ultimate bearing capacity, the calculation model in Fig.2(a) is taken as an example for the formula derivation. The depth range of reinforced materials and the relative position of the sliding zone will affect the ultimate bearing capacity of reinforced ground near slope. In Fig.2, the vertical distance from the deepest C point of the region I to footing bottom is H_1, and the effective reinforcement depth H_e is the vertical distance from the deepest point of failure slip line to footing bottom. It is assumed that all the reinforced materials are within the failure zone, that is, the distance from the bottom layer of reinforced material to footing bottom h_n is less than or equal to H_e. According to the relative size between h_n and H_1, H_e, two cases of $h_n\leqslant H_1$ and $H_1<h_n\leqslant H_e$ are discussed.

3.1.1 $h_n\leqslant H_1$

When $h_n\leqslant H_1=0.5B\tan(\pi/4+\varphi_t/2)$, the tensile force of reinforced materials acts on three parts of regions I, II, and III simultaneously. The stress state of each region as an isolation body is determined according to the factors including the force transfer relationship of region I→II→III, the relative sliding between adjacent regions, and the contributions of the soil cohesion and tensile force of reinforced materials to the ultimate bearing capacity of ground. However, the force analysis of the isolated body is carried out in the reverse order of the force transfer

relationship. Figure 4 shows the force analysis of the isolated body *BDEF*. From the force balance in the horizontal and vertical directions, we have

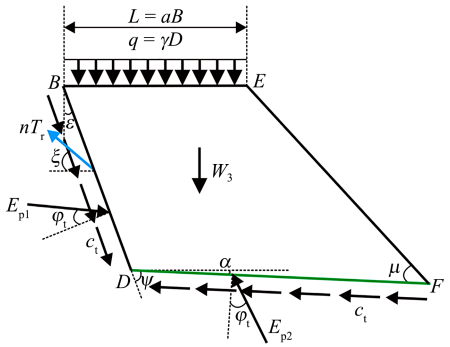

Fig. 4 Force analysis of the isolated body *BDFE*

$$E_{\mathrm{p1}}\cos(\varphi_{\mathrm{t}}-\varepsilon)+c_{\mathrm{t}}\overline{BD}\sin\varepsilon=E_{\mathrm{p2}}\sin(\varphi_{\mathrm{t}}-\alpha)+c_{\mathrm{t}}\overline{DF}\cos\alpha+nT_{\mathrm{r}}\sin\xi \tag{3}$$

$$qL+W_3+E_{\mathrm{p1}}\sin(\varphi_{\mathrm{t}}-\varepsilon)+c_{\mathrm{t}}\overline{BD}\cos\varepsilon=E_{\mathrm{p2}}\cos(\varphi_{\mathrm{t}}-\alpha)+c_{\mathrm{t}}\overline{DF}\sin\alpha+nT_{\mathrm{r}}\cos\xi \tag{4}$$

where E_{p1} and E_{p2} are the passive earth pressures on planes *BD* and *DF*, which act on $\overline{BD}/3$ and $\overline{DF}/3$ from point *D*, respectively, and the angle between their directions and the normal of the action surface is φ_{t}; ε is the included angle between the *BD* plane and the vertical line. According to the geometric relationship shown in Fig.2(a), it can be obtained that $\varepsilon=\varphi_{\mathrm{t}}/2+\theta-\pi/4$; and $W_3=\gamma S_3$ is the soil self-weight of the isolation body *BDFE*, S_3 is the area of the isolated body *BDFE*, which is expressed as follows:

$$S_3=\frac{1}{2}\overline{BD}\left(2L\cos\varepsilon-\frac{1}{2}\sin 2\varepsilon+\overline{BD}\frac{\cos^2\varepsilon}{\tan\eta}\right)+\frac{1}{2}\overline{DF}\left(L-\overline{BD}\sin\varepsilon+\overline{BD}\frac{\cos\varepsilon}{\tan\eta}\right)\sin\alpha \tag{5}$$

According to the geometric relationship in Fig.2(a), the length of *DF* is

$$\overline{DF}=\frac{L\sin\eta+\overline{BD}\cos(\varepsilon+\eta)}{\sin\mu} \tag{6}$$

Since *CD* is the logarithmic spiral, *BC* can be regarded as the initial radius. So, the length of *BD* is

$$\overline{BD}=\overline{BC}\mathrm{e}^{\theta\tan\varphi_{\mathrm{t}}}=\frac{B\mathrm{e}^{\theta\tan\varphi_{\mathrm{t}}}}{2\cos(\pi/4+\varphi_{\mathrm{t}}/2)} \tag{7}$$

where θ is the angle between *BD* and *BC*.

Since *DF* is the tangent of *CD* at point *D*, assuming that the angle between *DF* and the extension line of *BD* is ψ, then by the definition of the logarithmic spiral equation[39], it can be obtained:

$$\cot\psi=\tan\varphi_{\mathrm{t}} \tag{8}$$

Thus, we can get that ψ, α, and θ are respectively:

$$\psi=\frac{\pi}{2}-\varphi_{\mathrm{t}},\quad \alpha=\eta-\frac{\pi}{4}+\frac{\varphi_{\mathrm{t}}}{2},\quad \theta=\frac{\pi}{4}+\frac{\varphi_{\mathrm{t}}}{2}-\alpha \tag{9}$$

By combining Eq.(3) with Eq.(4), the passive earth pressure E_{p1} can be derived as

$$E_{\mathrm{p1}}=\frac{qL+W_3}{\cos\varphi_{\mathrm{t}}}\sin(\varphi_{\mathrm{t}}-\alpha)+c_{\mathrm{t}}\overline{DF}+nT_{\mathrm{r}}\sin(\xi+\alpha-\varphi_{\mathrm{t}}) \tag{10}$$

The force analysis of the isolated body *BCD* is shown in Fig.5. The following equation can be obtained by the moment equilibrium at point *B*:

$$\Sigma M_B=\int_0^{\theta}c_{\mathrm{t}}r^2\mathrm{d}\theta+\frac{2}{3}E_{\mathrm{p1}}\overline{BD}\cos\varphi_{\mathrm{t}}-\sum_{i=1}^{n}(T_{\mathrm{r}}h_i)\cdot\cos(\xi+\varphi_{\mathrm{t}}-\alpha)-\frac{2}{3}E_{\mathrm{p3}}\overline{BC}\cos\varphi_{\mathrm{t}}+W_2\lambda=0 \tag{11}$$

In Eq.(11)

$$\left.\begin{aligned}&\int_0^{\theta}c_{\mathrm{t}}r^2\mathrm{d}\theta=\frac{c_{\mathrm{t}}\overline{BC}^2}{2\tan\varphi_{\mathrm{t}}}(\mathrm{e}^{2\theta\tan\varphi_{\mathrm{t}}}-1),\\&W_2=\gamma S_2,\ S_2=\frac{\overline{BC}^2}{4\tan\varphi_{\mathrm{t}}}(\mathrm{e}^{2\theta\tan\varphi_{\mathrm{t}}}-1)\end{aligned}\right\} \tag{12}$$

where E_{p3} is the passive earth pressure on *BC*, which acts at $\overline{FG}/3$ away from point *C*, and the angle between its direction and the normal of action surface is φ_{t}; W_2 is the soil self-weight of the isolated body *BCD*; S_2 is the area of the isolated body *BCD*; and λ is the horizontal distance from W_2 to point *B*.

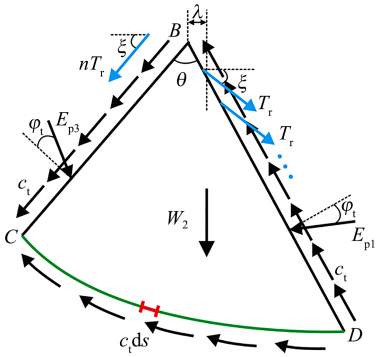

Fig. 5 Force analysis of the isolated body *BCD*

The passive earth pressure E_{p3} can be derived from Eq.(11):

$$E_{\mathrm{p3}}=\frac{3}{2}\frac{\int_0^{\theta}c_{\mathrm{t}}r^2\mathrm{d}\theta}{\overline{BC}\cos\varphi_{\mathrm{t}}}+\frac{\overline{BD}}{\overline{BC}}E_{\mathrm{p1}}+\frac{3}{2}\frac{W_2\lambda}{\overline{BC}\cos\varphi_{\mathrm{t}}}-\frac{3}{2}\frac{\sum_{i=1}^{n}(T_{\mathrm{r}}h_i)\cos(\xi+\varphi_{\mathrm{t}}-\alpha)}{\overline{BC}\cos\varphi_{\mathrm{t}}} \tag{13}$$

Figure 6 is a rectangular coordinate system with B as the origin and BC as the x-axis. Parameter λ is equal to

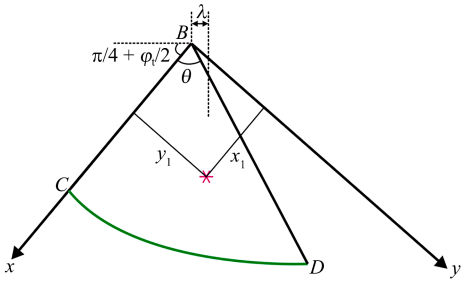

Fig. 6 Geometric parameters of the isolated body *BCD*

$$\lambda = y_1 \sin\left(\frac{\pi}{4}+\frac{\varphi_t}{2}\right) - x_1 \cos\left(\frac{\pi}{4}+\frac{\varphi_t}{2}\right) \tag{14}$$

$$x_1 = \frac{4\tan\varphi_t\left[e^{3\theta\tan\varphi_t}\left(\sin\theta+3\tan\varphi_t\cos\theta\right)-3\tan\varphi_t\right]}{3\left(1+9\tan^2\varphi_t\right)\left(e^{2\theta\tan\varphi_t}-1\right)}\overline{BC} \tag{15}$$

$$y_1 = \frac{4\tan\varphi_t\left[e^{3\theta\tan\varphi_t}\left(3\tan\varphi_t\sin\theta-\cos\theta\right)+1\right]}{3\left(1+9\tan^2\varphi_t\right)\left(e^{2\theta\tan\varphi_t}-1\right)}\overline{BC} \tag{16}$$

where (x_1, y_1) is the coordinate of the centroid of the sector isolated body BCD[39].

The stress analysis of the symmetrical half structure of the isolated body ABC is shown in Fig.7, and the equilibrium equation of its vertical force is

$$\frac{q_{ur}B}{2}+\frac{W_1}{2} = E_{p3}\cos\left(\frac{\pi}{4}-\frac{\varphi_t}{2}\right)+c_t\overline{BC}\sin\left(\frac{\pi}{4}+\frac{\varphi_t}{2}\right)+ nT_r\sin\xi \tag{17}$$

where $W_1 = \gamma S_1$ is the soil self-weight of the isolated body ABC, and S_1 is the area of the isolated body ABC, namely

$$S_1 = \frac{B^2}{4}\tan\left(\frac{\pi}{4}+\frac{\varphi_t}{2}\right) \tag{18}$$

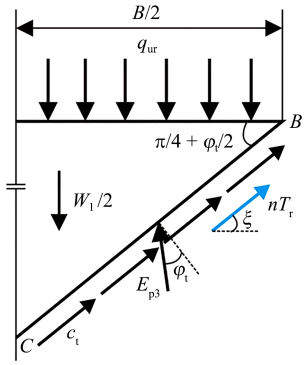

Fig. 7 Force analysis of the semi-structure of the isolated body *ABC*

By substituting Eq.(13) into Eq.(17), the ultimate bearing capacity of reinforced ground near slope under general shear failure mode can be obtained:

$$q_{ur} = q_u + \Delta q_u = c_t N_c + qN_q + \frac{1}{2}\gamma B N_\gamma + \Delta q_u \tag{19}$$

$$\left.\begin{aligned} N_c &= \tan\left(\frac{\pi}{4}+\frac{\varphi_t}{2}\right)+\frac{2}{B}\overline{DF}\cos\left(\frac{\pi}{4}-\frac{\varphi_t}{2}\right)e^{\theta\tan\varphi_t}+ \frac{3}{4}\tan\left(\frac{\pi}{4}+\frac{\varphi_t}{2}\right)\frac{e^{2\theta\tan\varphi_t}-1}{\sin\varphi_t} \\ N_q &= 2\frac{L}{B}\sin\left(\varphi_t-\alpha\right)\cos\left(\frac{\pi}{4}-\frac{\varphi_t}{2}\right)\frac{e^{\theta\tan\varphi_t}}{\cos\varphi_t} \\ N_\gamma &= 4S_3\sin\left(\varphi_t-\alpha\right)\cos\left(\frac{\pi}{4}-\frac{\varphi_t}{2}\right)\frac{e^{\theta\tan\varphi_t}}{B^2\cos\varphi_t}+ \frac{6S_2\lambda}{B^3}-\frac{2S_1}{B^2} \end{aligned}\right\} \tag{20}$$

$$\Delta q_u = \frac{2}{B}nT_r\sin\xi+\frac{3}{B^2}T_r\sum_{i=1}^{n}h_i\cos\left(\xi+\varphi_t-\alpha\right)+ 2nT_r\frac{e^{\theta\tan\varphi_t}}{B\cos\varphi_t}\cos\left(\frac{\pi}{4}-\frac{\varphi_t}{2}\right)\sin\left(\xi+\alpha-\varphi_t\right) \tag{21}$$

where q_u is the ultimate bearing capacity of non-reinforced ground near slope; N_c, N_q and N_γ are the bearing capacity coefficients of cohesion, overload and unit weight; Δq_u is the increment of ultimate bearing capacity of reinforced ground near slope caused by reinforced materials.

3.1.2 $H_1 < h_n \leqslant H_e$

When $H_1 < h_n \leqslant H_e$, the effective reinforcement depth H_e should be determined first. When $\alpha > 0$, the deepest point of the slip line is F in Fig.2(a), and the effective reinforcement depth H_e at this time is

$$H_e = \left(\overline{BD}\cos\varepsilon+\overline{DF}\sin\alpha\right)\cos\eta \tag{22}$$

When $\alpha \leqslant 0$, the deepest point of the slip line appears on the plane CD, corresponding to point G[12] directly below point B in Fig.2(b), and the effective reinforcement depth H_e at this time is

$$H_e = \overline{BG} = \overline{BC}\,e^{\theta_h\tan\varphi_t} = \frac{Be^{\theta_h\tan\varphi_t}}{2\cos\left(\pi/4+\varphi_t/2\right)} \tag{23}$$

where $\theta_h = \theta + \varphi_t/2 - \pi/4$ is the angle between BG and BC.

Since the tensile force of the reinforced materials within the range of $H_1 < h_n \leqslant H_e$ cannot function in the region I, the reinforcement effect shall be reduced. By taking the ratio of the depth H_1 of region I and the distance h_i from the reinforced material to the footing bottom as the reduction coefficient[12], the ultimate bearing capacity of the reinforced ground near slop under general shear failure mode q_{ur}, can be modified to

$$q_{\mathrm{ur}}=q_{\mathrm{u}}+\Delta q_{\mathrm{u}}'=c_{\mathrm{t}}N_c+qN_q+\frac{1}{2}\gamma BN_\gamma+\Delta q_{\mathrm{u}}' \tag{24}$$

$$\Delta q_{\mathrm{u}}'=\frac{2}{B}T_{\mathrm{r}}\sum_{i=1}^{n}R_{Ti}\sin\xi-\frac{3}{B^2}T_{\mathrm{r}}\sum_{i=1}^{n}\left(R_{Ti}h_i\right)\cos\left(\xi+\varphi_{\mathrm{t}}-\alpha\right)+$$

$$2T_{\mathrm{r}}\sum_{i=1}^{n}R_{Ti}\frac{\mathrm{e}^{\theta\tan\varphi_{\mathrm{t}}}}{B\cos\varphi_{\mathrm{t}}}\cos\left(\frac{\pi}{4}-\frac{\varphi_{\mathrm{t}}}{2}\right)\sin\left(\xi+\alpha-\varphi_{\mathrm{t}}\right) \tag{25}$$

where R_{Ti} is the reduction coefficient of reinforced material depth, and its expression is given as

$$R_{Ti}=\begin{cases}1, & \text{when } h_i\leqslant H_1\\ \dfrac{H_1}{h_i}, & \text{when } H_1<h_i\leqslant H_{\mathrm{e}}\end{cases} \tag{26}$$

When $h_n\leqslant H_1$, all the reinforced material meets the condition of $h_i\leqslant H_1$, then $R_{Ti}=1$. At this time, Eq.(24) degenerates into Eq.(19), that is, Eq.(19) can be regarded as a special case of Eq.(24). Therefore, Eq.(24) is the general formula for calculating the ultimate bearing capacity of reinforced ground near slope under general shear failure mode in this paper.

3.2 Composite failure

Previous research results in the literatures[13−14, 34, 40] show that the effective reinforced depths H_{e} of clay ground reinforced by geogrids and geotextiles are 1.5B and 1.25B, respectively, and the influence of reinforced materials can be ignored when $h_i>H_{\mathrm{e}}$. Assuming that the distance h_n between the bottom layer of reinforced materials and footing bottom is less than or equal to H_{e}. In the case of composite failure, the derivation of ultimate bearing capacity can be divided into the general shear failure zone including regions I, II and III, and the punching shear failure zone of region IV in Fig.3. The derivation process of the ultimate bearing capacity formula is the same in the two cases of $\alpha>0$ and $\alpha\leqslant 0$. Therefore, the calculation model in Fig.3(a) is used to deduce the formula of the ultimate bearing capacity of the reinforced ground near slope under the composite failure mode. The force analysis of the semi-structure of the isolated body $ABB'A'$ in Fig.3(a) is shown in Fig.8, and the equilibrium equation of its vertical force is

$$\frac{q_{\mathrm{ur}}B}{2}+\frac{W_4}{2}=\frac{q_{\mathrm{ub}}B}{2}+E_{\mathrm{p4}}\sin\varphi_{\mathrm{t}}+c_{\mathrm{t}}h_n+nT_{\mathrm{r}}\sin\xi \tag{27}$$

where $W_4=\gamma Bh_n$ is the soil self-weight of the isolated body $ABB'A'$; q_{ub} is the bearing capacity of plane $A'B'$ in Fig.3(a), that is, the ultimate bearing capacity of the soil in the general shear failure zone under reinforced material layers; E_{p4} is the passive earth pressure on the BB' plane, which can be determined according to Rankine's earth pressure theory[13−14], i.e.,

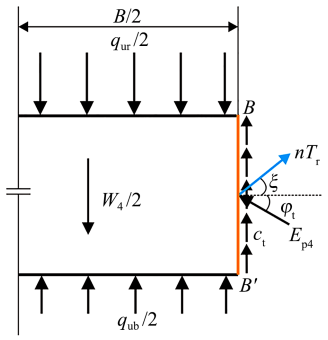

Fig. 8 Force analysis of the semi-structure in zone IV

$$E_{\mathrm{p4}}=2\left(c_{\mathrm{t}}+\gamma D\right)h_n\tan\left(\frac{\pi}{4}+\frac{\varphi_{\mathrm{t}}}{2}\right)+\frac{1}{2}\gamma h_n^2\tan^2\left(\frac{\pi}{4}+\frac{\varphi_{\mathrm{t}}}{2}\right) \tag{28}$$

The general shear failure zone under reinforced material layers is shown in Fig.9. The effect of soil self-weight on the $B'E'$ plane is simplified as the surcharge $q+\gamma h_n$, and the length of $B'E$ is $L'=L+h_n/\tan\eta$. The solution and analysis process of the bearing capacity of the $A'B'$ plane q_{ub} is similar to that in Section 3.1, but the effect of T_{r} should be removed. The bearing capacity of the $A'B'$ plane q_{ub} can be expressed as

$$q_{\mathrm{ub}}=c_{\mathrm{t}}N_c'+\left(q+\gamma h_n\right)N_q'+\frac{1}{2}\gamma BN_\gamma' \tag{29}$$

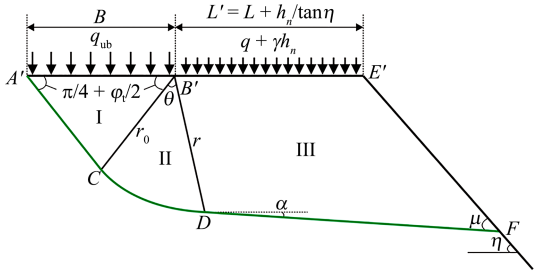

Fig. 9 General shear failure zone under reinforced material layers

$$\left.\begin{aligned}N_c'&=\tan\left(\frac{\pi}{4}+\frac{\varphi_{\mathrm{t}}}{2}\right)+\frac{2}{B}\left(\overline{DF}+\frac{h_n\cos\eta}{\sin\mu}\right)\cos\left(\frac{\pi}{4}-\frac{\varphi_{\mathrm{t}}}{2}\right)\mathrm{e}^{\theta\tan\varphi_{\mathrm{t}}}+\frac{3}{4}\tan\left(\frac{\pi}{4}+\frac{\varphi_{\mathrm{t}}}{2}\right)\frac{\mathrm{e}^{2\theta\tan\varphi_{\mathrm{t}}}-1}{\sin\varphi_{\mathrm{t}}}\\ N_q'&=2\frac{L+h_n/\tan\eta}{B}\sin\left(\varphi_{\mathrm{t}}-\alpha\right)\cos\left(\frac{\pi}{4}-\frac{\varphi_{\mathrm{t}}}{2}\right)\frac{\mathrm{e}^{\theta\tan\varphi_{\mathrm{t}}}}{\cos\varphi_{\mathrm{t}}}\\ N_\gamma'&=4S_3'\sin\left(\varphi_{\mathrm{t}}-\alpha\right)\cos\left(\frac{\pi}{4}-\frac{\varphi_{\mathrm{t}}}{2}\right)\frac{\mathrm{e}^{\theta\tan\varphi_{\mathrm{t}}}}{B^2\cos\varphi_{\mathrm{t}}}+\frac{6S_2\lambda}{B^3}-\frac{2S_1}{B^2}\end{aligned}\right\} \tag{30}$$

where S_3' is the area of the quadrilateral $B'DFE'$, and its expression is

$$S_3' = \frac{1}{2}\overline{BD}\left(2L'\cos\varepsilon - \frac{1}{2}\sin 2\varepsilon + \overline{BD}\frac{\cos^2\varepsilon}{\tan\eta}\right) + \frac{1}{2}\left(\overline{DF} + \frac{h_n\cos\eta}{\sin\mu}\right)\left(L' - \overline{BD}\sin\varepsilon + \overline{BD}\frac{\cos\varepsilon}{\tan\eta}\right)\sin\alpha \tag{31}$$

By substituting Eqs. (28) and (29) into Eq.(27), the ultimate bearing capacity of the reinforced ground near slope under composite failure mode can be obtained as follows:

$$q_{\mathrm{ur}} = c_{\mathrm{t}}N_c' + (q+\gamma h_n)N_q' + \frac{1}{2}\gamma BN_\gamma' + \frac{2}{B}E_{\mathrm{p4}}\sin\varphi_{\mathrm{t}} + \frac{2}{B}c_{\mathrm{t}}h_n + \frac{2}{B}nT_{\mathrm{r}}\sin\xi - \gamma h_n \tag{32}$$

The results of the model test conducted by Shin et al.[20] suggested that the ultimate bearing capacity of reinforced clay ground near slope q_{ur}, first increased and then decreased with the increase in the distance of top reinforced material layer u, and gradually decreased with increasing the vertical spacing between layers of reinforced materials z_i. In general, the ultimate bearing capacity of horizontally reinforced clay ground decreases with the increase of the vertical spacing between layers of reinforced materials[34, 40]. However, when the number of reinforced material layers n is constant, the bearing capacity q_{ur} in Eq.(32) increases with the increase of the distance between the bottom layer of reinforced materials and footing bottom (it is actually the distance of the top reinforced material layer u or the vertical spacing between layers of reinforced materials z_i), which is contrary to the influence characteristics of the vertical spacing between reinforced material layers. Therefore, the reduction coefficient s_u of u and the reduction coefficient s_{zi} of z_i in the literature[20] are introduced to comprehensively modify the increment term of ultimate bearing capacity caused by the effect of reinforced materials in Eq.(32). s_u and s_{zi} can be expressed as

$$s_u = \begin{cases} 0.32u/B + 0.87, & \text{when } u/B \leqslant 0.4 \\ 1.19 - 0.48u/B, & \text{when } 0.4 < u/B \leqslant 0.5 \end{cases} \tag{33}$$

$$s_{zi} = 1.3 - 0.9z_i/B, \ \text{when } z_i/B < 0.5 \tag{34}$$

After modification, the ultimate bearing capacity of reinforced ground near slope under composite failure mode q_{ur} is

$$q_{\mathrm{ur}} = c_{\mathrm{t}}N_c' + (q+\gamma h_n)N_q' + \frac{1}{2}\gamma BN_\gamma' + \frac{2}{B}E_{\mathrm{p4}}\sin\varphi_{\mathrm{t}} + \frac{2}{B}c_{\mathrm{t}}h_n + \frac{2}{B}T_{\mathrm{r}}\sin\xi\left(s_u + \sum_{i=2}^{n}s_{zi}\right) - \gamma h_n \tag{35}$$

3.3 Comparison of other methods

Based on the unified strength theory, novel solutions to the ultimate bearing capacity of reinforced ground near slope (i.e., Eq.(24) and Eq.(35)) are presented in this paper. In view of two modes of general shear failure and composite failure of reinforced ground, the effects of the intermediate principal stress ($0 \leqslant b \leqslant 1$), the vertical spacing between reinforced material layers z_i, the number of reinforced material layers n, and the tensile strength of reinforced material T_{u}, were comprehensively taken into consideration in the new solution, which has extensive theoretical significance.

When the tensile force of reinforced materials T_{r} and the distance between the bottom layer of reinforced materials and footing bottom h_n are 0, Eqs. (24) and (35) are equal and they are all the ultimate bearing capacity solutions of unreinforced ground near slope based on the unified strength theory. The unified strength theory parameter b represents different selections of strength criteria. When b = 0, Eqs. (24) and (35) degenerate into the ultimate bearing capacity solutions of reinforced ground near slope based on Mohr-Coulomb strength criterion. When b = 0, T_{r} = 0, h_n = 0, Eqs. (24) and (35) degenerate into the ultimate bearing capacity solution of unreinforced ground near slope based on Mohr-Coulomb strength criterion in the literature[39]. When b=1, Eqs. (24) and (35) are the ultimate bearing capacity solutions of reinforced ground near slope based on twin shear stress strength criterion. When $0<b<1$, a series of new ultimate bearing capacity solutions of reinforced ground near slope can be obtained from Eqs. (24) and (35).

Therefore, the new solutions to ultimate bearing capacity of reinforced ground near slope obtained in this paper can be degenerated into the solutions in the published literature, and a variety of unpublished new solutions can be obtained, which are suitable for different engineering practical situations.

3.4 Application steps

For reinforced sandy soil ground or clay ground near slope with $u \leqslant 0.5B$ and $z_i \leqslant 0.5B$, Eqs. (24) and (35) can be used to solve the ultimate bearing capacity of reinforced ground near slope. A strip footing with width B and buried depth D is given and placed near the slope with angle η. The horizontal distance from footing to slope shoulder is L, and the underlying ground is reinforced with n layers. The physical and mechanical indexes of foundation soil are known (unit weight γ, cohesion c and internal friction angle φ): (i) for sandy soil ground with $0.25B < u \leqslant 0.5B$ or $0.25B < z_i \leqslant 0.5B$, the ultimate bearing capacity of reinforced ground near slope can be solved according to Eq.(24); (ii) for sandy soil ground with u, $z_i \in (0, 0.25B]$ and clay foundation with u, $z_i \in (0, 0.5B]$, the ultimate

bearing capacity can be calculated by Eq.(35). The specific application steps are shown in Fig.10.

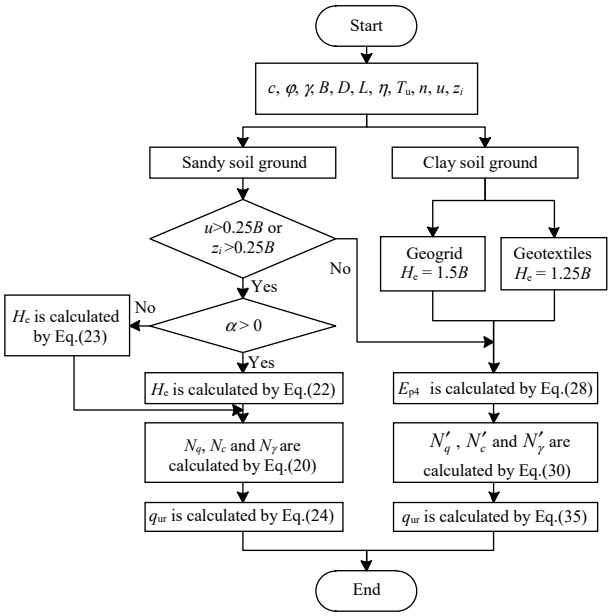

Fig. 10 Flowchart of application steps

4 Comparison of model tests

To verify the effectiveness of the new solutions, the calculation results of the new solution of the ultimate bearing capacity of the reinforced ground near slope under the general shear failure and composite failure modes (i.e., Eqs. (24) and (35)) in this paper are compared with the model test results in the literature[15, 18, 20], respectively.

4.1 General shear failure

In the literature[15], a strip footing was embedded in sandy slope, the ultimate bearing capacity of multi-layer reinforced sand soil ground below the footing was studied by model test. During the model test, the general shear failure occurred in the reinforced ground near slope. The measured value from the model test is compared with the calculated value based on Eq.(24) in this paper, as shown in Fig.11. The parameters used for the ground and reinforced materials are as follows: c = 0 kPa, φ = 42°, γ = 20 kN/m^3, B = 0.08 m, D = 0, a = 1.5, η = 34°, $u = z_i$ = 0.3B, T_u = 55 kN/m, RF_{CR} = 5, RF_{ID} = 3, RF_D = 2.

It can be seen from Fig.11 that the ultimate bearing capacity q_{ur} of reinforced ground near slope obtained from Eq.(24) and model test increase significantly with the increase of the number of reinforced layers n. When b = 0.5, the calculated value in this work is in good agreement with the measured value from the model test in the literature[15], and the average relative error between the two results is only 5.3%, which verifies the validity of Eq.(24) in this work and also suggests that the shear strength of the sand tested should be determined by Eq.(1) when

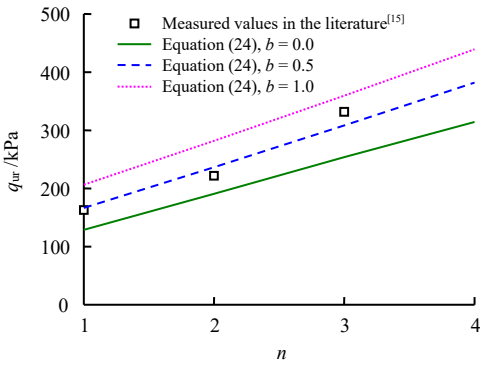

Fig. 11 Comparisons with the model test results from literature [15]

parameter b = 0.5. When b = 0, the calculated value in this paper is significantly less than the measured value in the literature[15], indicating that the Mohr-Coulomb strength criterion (b=0) underestimates the potential of ground bearing capacity because it does not consider the influence of intermediate principal stress. When b = 1, the calculated value in this paper is obviously greater than the measured value in the literature[15], which exaggerates the effect of intermediate principal stress on soil shear strength.

4.2 Composite failure

In the previous study[18], model tests were carried out on the reinforced sandy soil ground near slope, and the failure modes of the soil above, between and under the reinforced material layers were obtained. It is pointed out in the literature[18] that when $u = z_i$ = 0.25B, the failure mode of the ground under the reinforced layer is composite failure. The model test results are compared with the calculated values obtained from Eq.(35) in this paper, as shown in Fig.12. The relevant parameters are as follows: c = 0.03 kPa, φ = 38.36°, γ = 16 kN/m^3, B = 0.12 m, D = 0, a = 0, η = 23°, T_u = 1 532 kN/m, RF_{CR} = 5, RF_{ID} = 3, RF_D = 2.

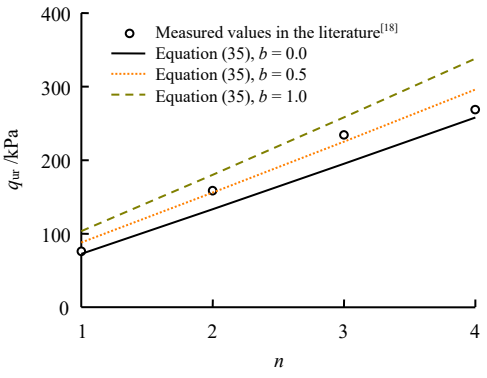

Fig. 12 Comparisons with the model test results from literature [18]

It can be seen from Fig.12 that when b = 0.5, the calculated value obtained from Eq.(35) is close to the measured value from the model test in the literature[18], and the average relative error of the two values is only 5.4%, which verifies the effectiveness of Eq.(35) in this work and also indicates that the shear strength of the sand tested should be determined by Eq.(1) when parameter b = 0.5. Additionally, when b = 0 (i.e., ignoring the effect of intermediate principal stress), the calculated value is smaller than the measured value from the model test and the calculated value in this work tends to be conservative. When b = 1, the calculated value is obviously larger than the measured value from the model test and the calculated value tends to be dangerous.

In the existing literature[20], the effect of reinforcement parameters on the ultimate bearing capacity of ground was studied by undrained model test of strip footing on the geogrid reinforced clay slope. The reinforced ground presented the characteristics of composite failure. The comparison between the measured value from the model test in the literature[20] and the calculated value determined by Eq.(35) in this paper is shown in Fig.13. The relevant parameters are as follows: c = 9.1 kPa, γ= 18.25 kN/m^3, B = 0.076 1 m, D = 0, a = 1, η = 45°; u = 0.4B, z_i = 0.333B, T_u = 182 kN/m, RF_{CR} = 5, RF_{ID} = 3, RF_D = 2. Since the internal friction angle φ in the undrained model test in literature[20] is 0°, but the expression of N_c' in Eq.(30) in this paper requires φ>0°, so φ = 0.01° was used for calculation in this work.

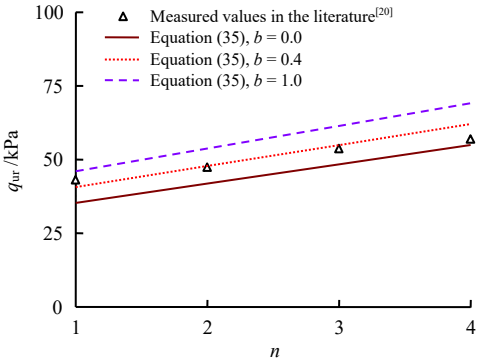

Fig. 13 Comparisons with the model test results from literature [20]

It can be observed from Fig.13 that when b=0.4, the calculated value obtained from Eq.(35) is consistent with the measured value from the model test on the reinforced clay ground in the literature[20], and the average relative error of the two values is only 4.8%, which verifies the validity of Eq.(35) in this work. Meanwhile, when the intermediate principal stress (b = 0) is not taken into account, the calculated value obtained from Eq.(35) is small, while the calculated value obtained from Eq.(35) is significantly large when b = 1.

5 Parameter analysis

The influences of the intermediate principal stress, the vertical spacing between reinforced material layers, the number of reinforced material layers and the tensile strength of reinforced materials on the ultimate bearing capacity of reinforced ground near slope are discussed. The parameter analysis of ultimate bearing capacity of the reinforced ground near slope under general shear failure mode, i.e., Eq.(24), adopts the model test parameters of sandy soil ground near slope in the literature[15] in Section 4.1. The parameter analysis for the composite failure mode, i.e., Eq.(35), adopts the model test parameters of clay ground in the literature[20] in Section 4.2.

5.1 Intermediate principal stress

The effect of intermediate principal stress on the shear strength of ground is obvious, and the unified strength theory parameter b can reflect the degree of the effect of intermediate principal stress. Figure 14 shows the variation of the ultimate bearing capacity q_{ur} of reinforced ground near slope with parameter b under the general shear failure and composite failure modes when the number of reinforced material layers n = 1, 2 and 3.

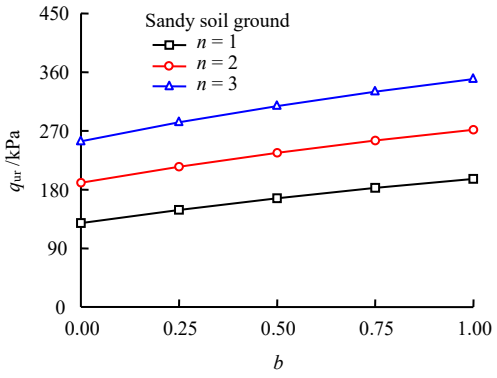

(a) General shear failure

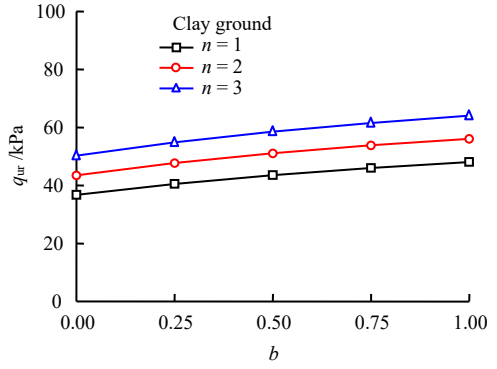

(b) Composite failure

Fig. 14 Influence of intermediate principal stress

The ultimate bearing capacity q_{ur} under the general shear failure and composite failure modes increase with the increase of parameter b. When the number of reinforced layers n = 1 and the parameter b increases from 0 to 1, the bearing capacity q_{ur} increases by 52.6% under general shear failure and 31.0% under composite failure, which shows that the intermediate principal stress prominently influence the ultimate bearing capacity of reinforced ground near slope. When b=0, the bearing capacity q_{ur} is obviously small because the effect of intermediate principal stress of foundation soil is not considered. The improvement of the ultimate bearing capacity of the reinforced ground by the intermediate principal stress should be considered to give full play to the strength potential of the foundation soil and reduce the project cost.

5.2 Vertical spacing between reinforcement layers

The distance h_n from the bottom reinforced material layer to the footing bottom varies with the change of vertical spacing between reinforced material layers z_i, and the ultimate bearing capacity of reinforced ground near slope also changes accordingly. Figure 15 shows the influence of vertical spacing z_i on the ultimate bearing capacity q_{ur} under general shear failure and composite failure modes, where the number of reinforced layers n = 3, and b = 0, 0.5 and 1. When $u \leqslant 0.25B$ and $z_i \leqslant 0.25B$, the ultimate bearing capacity of reinforced sandy soil ground near slope is calculated according to Eq.(35) under composite failure mode. When $0.25B < z_i \leqslant 0.5B$, the ultimate bearing capacity is calculated according to Eq.(24) under the general shear failure mode. In Fig.15(a), u is equal to $0.25B$.

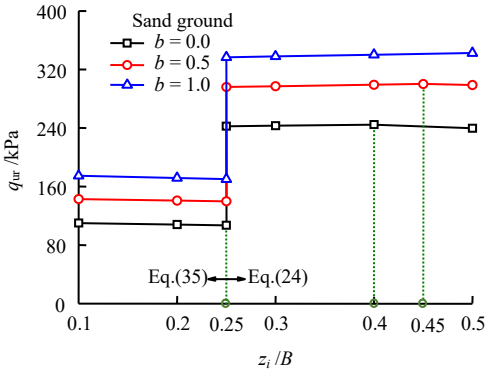

(a) Composite faulure →general shear failure

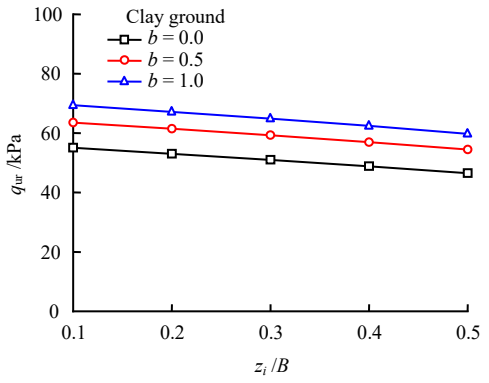

(b) Composite failure

Fig. 15 Influence of vertical spacing between reinforced material layers

When $0 \leqslant z_i < 0.25B$, the ultimate bearing capacity q_{ur} of reinforced sandy soil ground decreases with the increase of z_i under the composite failure mode. When $0.25B < z_i \leqslant 0.5B$, the effect of vertical spacing z_i between reinforced material layers on the reinforced sandy soil ground near slope under the general shear failure can be divided into two stages. That is, when $h_n \leqslant H_1$, the bearing capacity q_{ur} increases with the increase of z_i, and when $H_1 < h_n \leqslant H_e$, q_{ur} decreases with the increase of z_i. For example, in the case of b=0, the bearing capacity q_{ur} is decreased by 2.8% when z_i/B increases from 0.1 to 0.25; the bearing capacity q_{ur} under general shear failure is 1.27 times larger than that under composite failure when z_i/B = 0.25; when z_i/B increases from 0.25 to 0.4, $h_n \leqslant H_1$ = 0.078 m, and the bearing capacity q_{ur} is increased by 2.6%; when z_i/B increases from 0.4 to 0.5, $h_n > H_1$ = 0.078 m, and the bearing capacity q_{ur} is decreased by 3.6%. This is because under the general shear failure mode, the relative size between h_i and H_1 affects the reduction coefficient of the reinforced material depth, so that the bearing capacity first increases and then decreases, and the influence of the distance from the bottom layer of reinforced materials to footing bottom h_n is earlier and more prominent. In addition, the bearing capacity potential of the reinforced sandy soil ground near slope under composite failure can not be brought into full play. The vertical spacing between reinforced material layers should be reasonably controlled to avoid punching shear failure of reinforced soil ground.

It can be seen from Figure 15(b) that the ultimate bearing capacity q_{ur} under composite failure mode decreases with the increase of vertical spacing z_i, which is in line with the law observed from the model tests in the literature[20]. In the case of b = 0, the bearing capacity q_{ur} when z_i/B = 0.5, decreases by 15.6% compared with that when z_i/B = 0.1. Therefore, the vertical spacing between reinforced material layers has a certain influence on the ultimate bearing capacity q_{ur} under composite failure.

5.3 Number of reinforced material material layers

The variation of the number of reinforced material layers n also represents the variation of the distance from the reinforced material layers to footing bottom h_i. Figure 16 shows the influence of n on the ultimate bearing capacity q_{ur} under general shear failure and composite failure modes, where b = 0, 0.5, and 1. As geogrid reinforcement was employed in the literature[20], the effective reinforcement depth H_e = 1.5B is taken in Fig.16(b).

The case of b=0 in Fig.16(a) is analysed as an example

here. As the number of reinforced material layers n increases, the ultimate bearing capacity q_{ur} of the reinforced sandy soil ground near slope under general shear failure can be divided into three stages: (i) n increases from 1 to 4, the bearing capacity q_{ur} is increased by 1.44 times. At this time, $h_n \leqslant H_1$, and the bearing capacity q_{ur} increases linearly with the increase of n. (ii) n increases from 4 to 8, the bearing capacity q_{ur} is increased by 51.3%. At this time, $H_1 < h_n \leqslant H_e$, and the growth rate of bearing capacity q_{ur} decreases gradually, because when $h_i > H_1$, the reduction coefficient of reinforced material depth $R_{Ti} < 1$, and the reinforcement effect is weakened. (iii) When $n > 8$, the bearing capacity q_{ur} remains the same value as that when $n = 8$ with the increase of n. In this case, $h_n > H_e$, and the reinforcement effect of reinforced materials located in range of $h_i > H_e$ is not included.

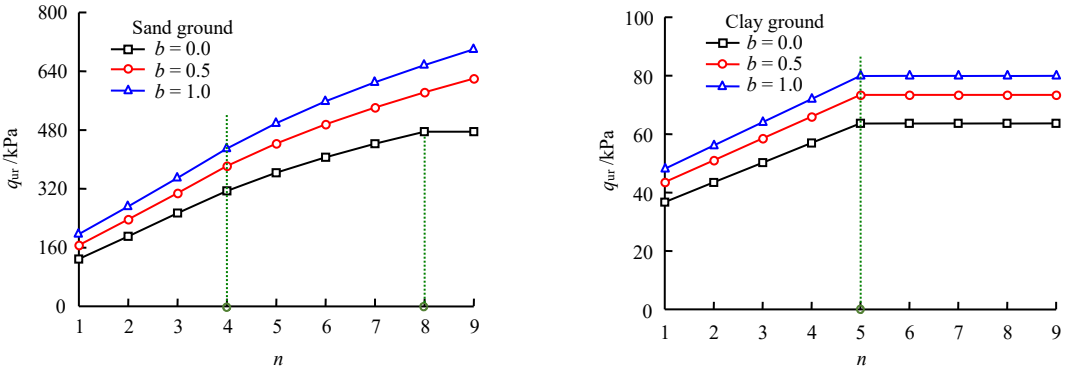

(a) General shear failure (b) Composite failure

Fig. 16 Influence of the number of reinforced material layers

With the increase of the number of reinforced material layers n, the ultimate bearing capacity q_{ur} of the reinforced clay ground near slope under composite failure can be divided into two stages: (i) When $b = 0$, and n increases from 1 to 5, the bearing capacity q_{ur} is increased by 73.4%. At this time, h_n is less than or equal to $H_e = 1.5B$, and the bearing capacity q_{ur} increases linearly with the increase of n. (ii) When $n > 5$, corresponding to $h_n > H_e$, only the reinforcement effect within the range of H_e is considered, and the bearing capacity q_{ur} remains unchanged. The number of reinforced material layers should be reasonably determined according to the effective depth of reinforced materials to reduce economic costs.

5.4 Tensile strength of reinforced materials

In the design of ground reinforcement, the tensile strength of reinforced materials is an important basis for the selection of reinforced material types. Figure 17 shows the influence of tensile strength of reinforced materials T_u on the ultimate bearing capacity q_{ur} of the reinforced ground near slope under general shear failure and composite failure modes, where the number of reinforced layers $n = 3$, and $b = 0$, 0.5, and 1.

It can be seen from Fig.17 that the ultimate bearing capacity q_{ur} of reinforced ground near slope under general shear failure and composite failure modes increases linearly with the increase of tensile strength of reinforced material T_u. In the case of $b = 0.5$, when T_u increases from 30 kN /m to 150 kN /m, the bearing capacity q_{ur} increases by 2.1 times and 32.8% under general shear failure and composite failure, respectively. Therefore, the tensile strength of reinforced materials has an important influence on the ultimate bearing capacity of reinforced ground near slope. The economic cost of the reinforced materials with high tensile strength is higher, so the type of reinforced materials should be selected reasonably according to the design requirements.

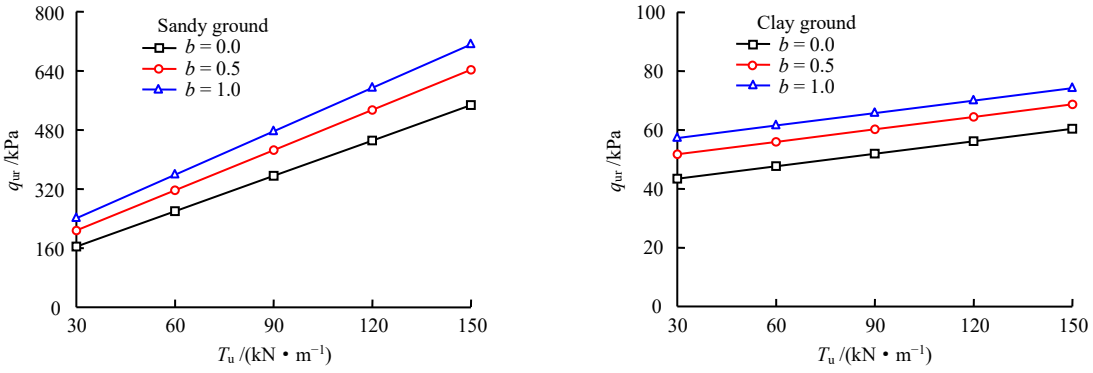

(a) General shear failure (b) Composite failure

Fig. 17 Influence of reinforced material tensile strength

6 Conclusions

(1) Aiming at two failure modes of general shear failure and composite failure of reinforced ground, new solutions of ultimate bearing capacity for reinforced ground near slope reasonably consider common effects of the intermediate principal stress, the vertical spacing between reinforced material layers, the number of reinforced material layers and the tensile strength of reinforced materials and have wide applicability. The effectiveness of the solution in this paper is verified by comparing with three groups of model test results from the literatures. At the same time, the ultimate bearing capacity solution of unreinforced ground near slope based on Mohr-Coulomb strength criterion in the literature[39], the ultimate bearing capacity solution of reinforced ground near slope based on Mohr Coulomb strength criterion and twin shear stress strength criterion are special cases of this work.

(2) The intermediate principal stress significantly influences the ultimate bearing capacity of the reinforced ground near slope under general shear failure and composite failure modes. The bearing capacity obtained without considering the intermediate principal stress is obviously small. Additionally, the ultimate bearing capacity of the reinforced ground near slope under general shear failure and composite failure modes increases significantly with the increase of the tensile strength of reinforced materials.

(3) The ultimate bearing capacity of the reinforced ground near slope under general shear failure first increases and then decreases with the increase of vertical spacing between reinforced material layers, which is related to the distance from the bottom reinforced material layer to the bottom of foundation. The ultimate bearing capacity of the reinforced ground near slope under composite failure decreases monotonically with the increase of vertical spacing between reinforced material layers. The vertical spacing of reinforced materials in sandy soil ground near slope should be reasonably controlled to avoid composite failure.

(4) Only the effect of effective reinforcement depth within the range can be counted. With the increase of the number of reinforced material layers, the ultimate bearing capacity of reinforced ground near slope increases linearly first, then slowly increases and finally remains unchanged under general shear failure. Under composite failure, the ultimate bearing capacity first increases and then remains unchanged, which is related to the distance from the bottom reinforced material layer to footing bottom.

References

[1] OUYANG Zhong-chun. Modern geotechnical reinforcement techniques[M]. Beijing: China Communications Press, 1991.

[2] WANG Zhao, WANG Xie-qun. Limit analysis for reinforced foundations[J]. Journal of Tsinghua University (Science and Technology), 2001, 41(6): 112−114.

[3] OURIA A, MAHMOUDI A, SADEGHPOUR H. Effect of the geotextile arrangement on the bearing capacity of a strip footing[J]. International Journal of Geosynthetics and Ground Engineering, 2020, 6(3): 1−14.

[4] ZHANG L L, WANG J Q, KALIAKIN V N, et al. Load-bearing characteristics of square footing on geogrid-reinforced sand subjected to repeated loading[J]. Journal of Central South University, 2020, 27(3): 920−936.

[5] LI Chi, WANG Jian-hua. Model testing study and calculating analysis of bearing capacity on the reinforced aeolian sands ground[J]. Chinese Journal of Rock Mechanics and Engineering, 2005, 24(4): 687−691.

[6] ZHOU Jian, KONG Xiang-li, WANG Xiao-cun. Bearing capacity behaviours and failure modes of reinforced grounds[J]. Chinese Journal of Geotechnical Engineering, 2008, 30(9): 1265−1269.

[7] BAI Chong-xi, ZHANG Zhong-hao, SHAO Xin-yan. An experimental study of strip foundation on the grounds reinforced with horizontal FRP[J]. Rock and Soil Mechanics, 2015, 36(4): 953−957.

[8] YAMAMOTO K, KUSUDA K. Failure mechanisms and bearing capacities of reinforced foundations[J]. Geotextiles and Geomembranes, 2001, 19(3): 127−162.

[9] LATHA G M, SOMWANSHI A. Bearing capacity of square footings on geosynthetic reinforced sand[J]. Geotextiles and Geomembranes, 2009, 27(4): 281−294.

[10] LIANG Bo, YANG You-hai. Theory and experiment on bearing capacity of reinforced sandy soil[J]. Chinese Journal of Geotechnical Engineering, 2008, 30(1): 123−127.

[11] LIU Shuan-qi, LU Kun-lin, ZHU Da-yong, et al. A method for calculating the ultimate bearing capacity of a strip footing on the reinforced sand[J]. Rock and Soil Mechanics, 2015, 36(8): 2307−2314.

[12] CAO Wen-gui, TAN Jian-hui, HU Wei-dong. Upper bound of ultimate bearing capacity for the reinforced grounds[J]. Rock and Soil Mechanics, 2018, 39(6): 1955−1962.

[13] SHARMA R, CHEN Q, ABU-FARSAKH M Y, et al. Analytical modeling of geogrid reinforced soil foundation[J]. Geotextiles and Geomembranes, 2009, 27(1): 63−72.

[14] CHEN Q, ABUFARSAKH M Y. Ultimate bearing capacity analysis of strip footings on reinforced soil foundation[J]. Soils and Foundations, 2015, 55(1): 74−85.

[15] YOO C. Laboratory investigation of bearing capacity behavior

of strip footing on geogrid-reinforced sand slope[J]. Geotextiles and Geomembranes, 2001, 19(5): 279−298.

[16] KESKIN M S, LAMAN M. Experimental and numerical studies of strip footings on geogrid-reinforced sand slope[J]. Arabian Journal for Science and Engineering, 2014, 39(3): 1607−1619.

[17] BAAH-FREMPONG E, SHUKLA S K. Behaviour of a strip footing embedded in a sand slope reinforced with multilayer geotextile[J]. Indian Geotechnical Journal, 2020, 50(4): 560−576.

[18] MA Qing-hong, ZHU Da-yong, LEI Xian-shun, et al. Laboratory modelling test on bearing capacity of reinforced sand slopes[J]. Chinese Journal of Geotechnical Engineering, 2014, 36(7): 1271−1280.

[19] SOMMERS A, VISWANADHAM B V. Centrifuge model tests on the behavior of strip footing on geotextile-reinforced slopes[J]. Geotextiles and Geomembranes, 2009, 27(6): 497−505.

[20] SHIN E C, DAS B M. Ultimate bearing capacity of strip foundation on geogrid-reinforced clay slope[J]. KSCE Journal of Civil Engineering, 1998, 2(4): 481−488.

[21] HALDER K, CHAKRABORTY D. Influence of soil spatial variability on the response of strip footing on geocell-reinforced slope[J]. Computers and Geotechnics, 2020, 122: 103533.

[22] JHA J N, CHOUDHARY A K, GILL K S, et al. Bearing capacity of a strip footing resting on reinforced fly ash slope: an analytical approach[J]. Indian Geotechnical Journal, 2013, 43(4): 354−366.

[23] LUO Ya-qiong, ZHANG Chao, MA Ting-ting. Solution for bearing capacity of multi-slide ground adjacent slope based on upper limit analysis[J]. Highway Engineering, 2019, 44(3): 97−101.

[24] KUMAR A, SARAN S. Bearing capacity of rectangular footing on reinforced soil[J]. Geotechnical and Geological Engineering, 2003, 21(3): 201−224.

[25] HALDER K, CHAKRABORTY D. Effect of inclined and eccentric loading on the bearing capacity of strip footing placed on the reinforced slope[J]. Soils and Foundations, 2020, 60(4): 791−799.

[26] JIANG Jing-shan, ZUO Yong-zhen, CHENG Zhan-lin, et al. Effects of stress state on mechanical properties of coarse granular material using large-scale true triaxial tests[J]. Rock and Soil Mechanics, 2020, 41(11): 3563−3572.

[27] YANG Ai-wu, YANG Shao-peng, LANG Rui-qing, et al. Three-dimensional mechanical properties of light solidified saline soil[J]. Rock and Soil Mechanics, 2021, 42(3): 593−600.

[28] YU Mao-hong. Unified strength theory for geomaterials and its applications[J]. Chinese Journal of Geotechnical Engineering, 1994, 16(2): 1−10.

[29] YU M H. Unified strength theory and its applications[M]. Berlin, Heidelberg: Springer, 2004.

[30] FAN Wen, BAI Xiao-yu, YU Mao-hong. Formula of ultimate bearing capacity of shallow foundation based on unified strength theory[J]. Rock and Soil Mechanics, 2005, 26(10): 1617−1622.

[31] GAO Jiang-ping, YU Mao-hong, LI Si-ping. Double-shear unified solution of Terzaghi ultimate bearing capacity of foundation[J]. Chinese Journal of Rock Mechanics and Engineering, 2005, 24(15): 2736−2740.

[32] MA Z Y, LIAO H J, DANG F N. Influence of intermediate principal stress on the bearing capacity of strip and circular footings[J]. Journal of Engineering Mechanics, 2014, 140(7): 04014041.

[33] DENG L S, FAN W, YU B, et al. Influence of the unified strength theory parameters on the failure characteristics and bearing capacity of sand foundation acted by a shallow strip footing[J]. Advances in Mechanical Engineering, 2020, 12(2): 1−13.

[34] CHEN Q, ABU-FARSAKH M, SHARMA R, et al. Laboratory investigation of behavior of foundations on geosynthetic-reinforced clayey soil[J]. Transportation Research Record, 2007, 2004(1): 28−38.

[35] ZHANG Chang-guang, CAI Ming-ming, QI Hang, et al. A unified solution for calculating mine backfills considering the backfilling order and the back wall cohesion[J]. Chinese Journal of Rock Mechanics and Engineering, 2019, 38(2): 226−236.

[36] CHEN Rong, LUAN Mao-tian, HAO Dong-xue, et al. The ultimate bearing capacity of reinforced foundation by variational solution[J]. Chinese Journal of Geotechnical Engineering, 2010, 32(5): 774−779.

[37] ZOU Wei-lie, WANG Zhao, LIN Xiao-ling. Creep reduction factor of geosynthetics[J]. Rock and Soil Mechanics, 2004, 25(12): 1961−1963, 1968.

[38] HOLTZ R D, CHRISTOPHER B R, BERG R R. FHWA-HI-98-038 Geosynthetic design and construction guidelines[S]. Washington: Federal Highway Administration, 1998.

[39] WANG Hong-yu, YANG Min. An estimate for the loss of bearing capacity of the footing near excavations[J]. China Civil Engineering Journal, 2005, 38(8): 99−105.

[40] YETIMOGLU T, WU J T H, SAGLAMER A. Bearing capacity of rectangular footings on geogrid-reinforced sand[J]. Journal of Geotechnical Engineering, 1994, 120(12): 2083−2099.